

Towards Emotion Analysis in Short-form Videos: A Large-Scale Dataset and Baseline

Xuecheng Wu¹, Heli Sun^{1‡}, Junxiao Xue², Jiayu Nie¹, Xiangyan Kong³, Ruofan Zhai⁴, Liang He¹

¹School of Computer Science and Technology, Xi'an Jiaotong University, Xi'an, China

²Research Center for Space Computing System, Zhejiang Lab, Hangzhou, China

³School of Electronics and Information Engineering, Harbin Institute of Technology, Harbin, China

⁴School of Cyber Science and Engineering, Zhengzhou University, Zhengzhou, China

wuxc3@stu.xjtu.edu.cn, hlsun@xjtu.edu.cn

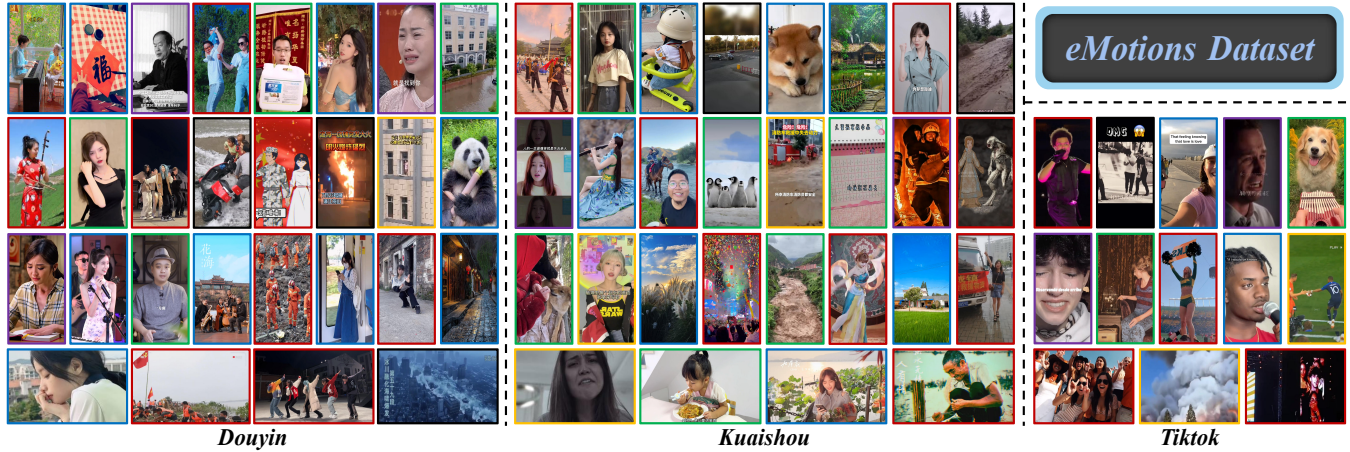


Figure 1: An overview of eMotions composed of 27,996 videos of six emotions across Douyin, Kuaishou, and Tiktok. The colors of frame borders specify the emotional categories to which they belong: *Excitation*, *Fear*, *Neutral*, *Relaxation*, *Sadness*, *Tension*.

ABSTRACT

Nowadays, short-form videos (SVs) are essential to web information acquisition and sharing in our daily life. The prevailing use of SVs to spread emotions leads to the necessity of conducting video emotion analysis (VEA) towards SVs. Considering the lack of SVs emotion data, we introduce a large-scale dataset named eMotions, comprising 27,996 videos. Meanwhile, we alleviate the impact of subjectivities on labeling quality by emphasizing better personnel allocations and multi-stage annotations. In addition, we provide the category-balanced and test-oriented variants through targeted data sampling. Some commonly used videos, such as facial expressions, have been well studied. However, it is still challenging to analysis the emotions in SVs. Since the broader content diversity brings more distinct semantic gaps and difficulties in learning emotion-related features, and there exists local biases and collective information gaps caused by the emotion inconsistency under the prevalently audio-visual co-expressions. To tackle these challenges, we present an end-to-end audio-visual baseline AV-CANet which

employs the video transformer to better learn semantically relevant representations. We further design the Local-Global Fusion Module to progressively capture the correlations of audio-visual features. The EP-CE Loss is then introduced to guide model optimization. Extensive experimental results on seven datasets demonstrate the effectiveness of AV-CANet, while providing broad insights for future works. Besides, we investigate the key components of AV-CANet by ablation studies. Datasets and code will be fully open soon.

CCS CONCEPTS

• **Information systems** → **Multimedia information systems**; • **Computing methodologies** → **Neural networks**.

KEYWORDS

Emotion analysis, Short-form videos, Dataset, Audio-visual learning

ACM Reference Format:

Xuecheng Wu¹, Heli Sun^{1‡}, Junxiao Xue², Jiayu Nie¹, Xiangyan Kong³, Ruofan Zhai⁴, Liang He¹. 2025. Towards Emotion Analysis in Short-form Videos: A Large-Scale Dataset and Baseline. In *Proceedings of the ACM Web Conference 2025 (WWW '25)*. ACM, New York, NY, USA, 10 pages. <https://doi.org/XXXXXXXX.XXXXXXX>

1 INTRODUCTION

Video emotion analysis (VEA) aims to mine the meanings of elements and uncover which emotion the elements evoke to the viewers. Meanwhile, the emotions of viewers can be influenced by various elements, such as videos, audio, and text from web media

Permission to make digital or hard copies of all or part of this work for personal or classroom use is granted without fee provided that copies are not made or distributed for profit or commercial advantage and that copies bear this notice and the full citation on the first page. Copyrights for components of this work owned by others than ACM must be honored. Abstracting with credit is permitted. To copy otherwise, or republish, to post on servers or to redistribute to lists, requires prior specific permission and/or a fee. Request permissions from permissions@acm.org.

WWW '25, April 28-May 02, 2025, Sydney, Australia

© 2025 Association for Computing Machinery.

ACM ISBN 979-8-4007-XXXX-X/25/05...\$15.00

<https://doi.org/XXXXXXXX.XXXXXXX>

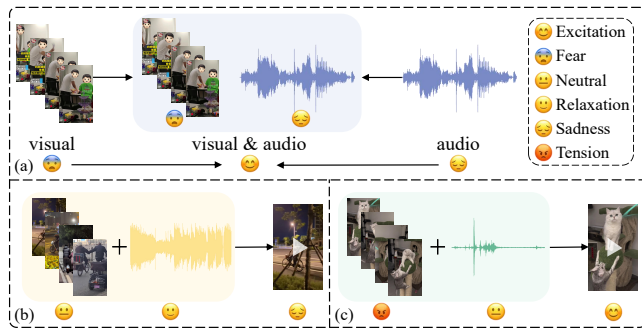


Figure 2: The overall illustration of emotion inconsistency. (a) Separate visual or auditory modality evokes different emotion, leading to expression conflict. (b)&(c) The lack of emotional information evoked from visual or auditory modality results in emotion disalignment.

[27], facilitating the developments of multi-modal VEA. Particularly, short-form videos¹ (SVs), one of the new types of social-media tools, have made rapid progress in recent years. SVs are concise and clear, combining visual, auditory, and other elements to intensify emotional expressions and arouse emotional resonance among viewers, which are crucial to spreading emotions. As a result, conducting VEA towards SVs has remarkable application values in research fields such as opinion mining [45] and dialogue systems [43].

Although VEA in facial expressions [54, 59] have been well studied, the research in SVs remains light because of the lack of large-scale dataset. To tackle this issue and facilitate further studies, we propose a dataset specifically constructed for emotion analysis in SVs, termed eMotions (Fig. 1), which is the first large-scale dataset in this field. eMotions consists of 27,996 videos with corresponding audio from Douyin, Kuaishou, and Tiktok three SVs platforms, covering various contents across diverse dimensions and totaling almost 198 hours of durations. Specifically, considering the discrete emotional categories in psychology and the content distribution characteristics of eMotions, we label each sample using the six emotional categories proposed by Plutchik in [35] (*i.e.*, Excitement, Fear, Neutral, Relaxation, Sadness, Tension). Moreover, to alleviate the impact of subjectivities on labeling quality, we elaborately adjust the personnel allocations through proposed two-stage Cross-Check and consistencies evaluations, as well as introduce a multi-stage annotation workflow. In addition, catering to the class distribution of eMotions and the testing demands, we provide the category-balanced and test-oriented variant datasets.

VEA towards SVs features the following challenges: As displayed in Fig. 1, the content diversity in SVs is broader, which leads to more distinct semantic gaps and barriers of learning emotion-related features than commonly used videos. Meanwhile, there exists emotion inconsistency under the prevalent audio-visual co-expressions, as shown in Fig. 2. Therefore, at local-level, inconsistency of emotion evocations with difficulties in integrating information lead to biases in model learning. Additionally, at global-level, the obstacles in emotion understanding within the overall feature space and accumulation of local biases result in more collectively significant information gaps. Considering these observations, we analyze

three keypoints as follows: (1) Learning more semantically relevant representations and emotion-related features in an end-to-end manner. (2) Interactive correlated modeling of inter-modalities at local-level, followed by selective integrations. (3) Supplementally facilitating complementary modeling of audio-visual correlations at global-level, while learning more contextual representations.

Based on these keypoints, we present an end-to-end audio-visual method denoted AV-CANet (Audio-Visual Cooperatively enhanced Analysis Network) as the baseline on proposed eMotions dataset. Unlike previous CNNs-based VEA methods [65, 68], we employ Video Swin-Transformer [30] as the visual backbone, which makes AV-CANet naturally capture the global relations between regions in each frame and efficiently model the long-range dependencies as well as long-term sequences, leading to more semantically relevant representations. The Local-Global Fusion Module (LGF Module) is designed to mitigate the local biases and collective information gaps, which progressively captures the correlated information of inter-modalities to output more comprehensive representations, as displayed in Fig. 6. Besides, we propose the EP-CE Loss (Emotion Polarity enhanced Cross-Entropy Loss), which incorporates three emotion polarities (*i.e.*, positive, neutral, negative) to guide model focusing more emotion-related features. The proposed method achieves superior performance in comparisons with advanced VEA baselines across three eMotions-related and four public datasets, indicating that it has the capability to benchmark eMotions.

In addition to VEA, the abundant emotions conveyed in eMotions can facilitate the research in LLMs (*e.g.*, multi-modal alignments with the emotional behaviors of humans [10]), emotional content generation [58], and explainable emotional reasoning [26]. Our main contributions are three-fold: (1) To our knowledge, eMotions is the first large-scale dataset for VEA towards SVs. The more reliable annotated emotions can promote the developments of affective content analysis. (2) We propose the baseline AV-CANet to analysis emotions in SVs. We design corresponding components to alleviate the impact of emotion inconsistency from local to global, and leverage the emotion-polarity information to better guide model optimization. (3) We conduct extensive experiments to verify the superiority of AV-CANet and provide detailed insights into different modalities and VEA datasets for future research. Ablations are also performed to investigate the key factors of our method.

2 RELATED WORKS

2.1 Video Emotion Analysis Datasets

Numerous datasets have emerged to facilitate the developments of VEA. FABO [12] consists of 1.9k videos of facial and body expressions recorded by cameras. IEMOCAP [4], the earliest audio-visual VEA dataset, originates from lab shooting. AFEW [8] contains 1,426 videos of 330 subjects labeled with seven emotions. Aff-Wild2 [20] includes 558 videos with annotations for valence-arousal estimations. VideoEmotion8 [18] and Ekman6 [55] consist of 1,101 and 1,637 videos drawn from video sites. CMU-MOSEI [62] comprises 23,500 YouTube-sourced utterances categorized under six emotions. CAER [23] and MELD [37] include 13,201 and 13,708 TV shows-derived clips, respectively. Music_video [33] houses 3,323 music recording videos labeled across six emotions. DFEW [17]

¹https://en.wikipedia.org/wiki/Video_clip#Short-form_videos

consists of 16,372 clips from thousands of movies under seven emotions. MAFW [28] is a compound affective facial database, including 10,045 video clips. MER2024 [25] encompasses 5,030 labeled and 115k unlabeled videos across six emotions, setting up three subsets. Compared with these datasets, our eMotions presents the following features: (1) The first large-scale dataset for VEA towards SVs, and the currently largest audio-visual VEA dataset with full video-level annotations. (2) An emphasis on better personnel allocations and multi-stage annotations to reduce the influence of subjectivities on labeling quality, engaging 12 annotators and one expert. (3) The larger extent of content diversity, covering a multi-cultural spectrum and spanning an extensive timeline of 45 months. (4) We additionally provide two variants of eMotions for diverse needs.

2.2 Video Emotion Analysis Methods

Early studies on VEA mainly center on designing hand-crafted features [14, 18]. With the emergence of various VEA datasets, methods based on deep learning have made rapid progress. For the uni-modal methods, [66] proposes a framework consisting of the CS-Former and T-Former branches. [57] presents a coarse-to-fine cascaded network with smooth predictions. Zhao et al. [67] introduces CLIP [40] and learnable tokens to enhance model performance. Regarding the audio-visual VEA approaches, [63] proposes a temporal erasing network for keyframe and context perceptions. [65] implements multiple attention mechanisms to output improved audio-visual features. [32] designs an intra-modality attention module to shape more refined features. [46] proposes a lightweight cross-modal fusion module that emphasizes more contributive features. [50] provides an audio-visual pre-trained framework to model the interactions between human facial and auditory behaviors. [39] introduces a joint model to extract salient features across audio-visual modalities. [34] and [56] introduce on-the-fly gradient modulation and a novel cosine loss for performance gains, respectively. [6] proposes a new model for incomplete audio-visual data. [36] presents an LSTM-based model to capture context-dependent semantics. [64] introduce a MAE-style VEA method via masking. [42] integrates the visual features extracted by the teacher-student networks with audio features using model-level fusion. In this work, we present AV-CANet to targetedly tackle the inherent challenges posed by the eMotions dataset, delivering superior performance across three eMotions-related and four public VEA datasets.

3 DATASET CONSTRUCTION

The overall construction pipeline of eMotions is shown as Fig. 3 (a), involving data collection and cleaning (Sec. 3.1), personnel assignment and adjustments (Sec. 3.2), multi-stage manual annotation and expert re-review (Sec. 3.3). We then present the labeling quality evaluations and dataset characteristics (Sec. 3.4 & 3.5). Besides, we provide the details of data selections for two variants (Sec. 3.6).

3.1 Data Collection and Cleaning

We collect hot events, which are diverse and representative, as the raw data. Meanwhile, we carry out a stage-by-stage crawling strategy interleaved with the formal annotation process to ensure a broad timeline. Besides, we extensively comply with the ethical considerations in terms of collection, privacy and data protections.

During data cleaning, identical and corrupted videos are first removed. The videos containing racial discrimination, violence, and pornography are then eliminated through machine detection and manual review to reduce the ethical biases of trained models. Furthermore, considering the specificities of discrete emotions, videos featuring consecutive emotional shifts are also discarded. More details are provided in the appendix.

3.2 Personnel Assignment and Adjustments

Each annotator is asked first to pass the labeling test, comprising the sentiment quotient test and the annotation quality evaluation [27, 60]. When scoring 90 or above in accuracy, the annotators can join in the emotion labeling. We then hold training sessions for them, including the detailed introduction of annotation workflow and targeted learning on multi-cultures.

Assignment: As formulated in Eq. 1, we empirically consider five key factors and set their coefficients to determine the assignment of group members and leaders. We also balance the gender distribution by allocating two males and one female for each group.

$$p = \alpha_1 \cdot we + \alpha_2 \cdot ms + \alpha_3 \cdot (eb + cb + lp), \quad (1)$$

where we , eb , cb , and lp respectively refer to the work experiences, education backgrounds, cultural backgrounds, and leaderships, which are all quantified using scoring tests. For MSCEIT [31] scores (ms), higher ranking indicates better emotional cognition. α_i ($i \in \{1, 2, 3\} = \{0.4, 0.3, 0.1\}$) are weight coefficients, respectively.

Adjustments: We perform personnel adjustments following assignment to alleviate the impact of subjectivities on the annotation workflow employing multi-groups with multi-annotators, which are reflected in the improvements of the consistencies of intra-group and inter-group (*i.e.*, S_a , S_r) [22]. Specifically, we select 9,000 samples from the cleaned data and distribute them evenly among the assigned groups. GroupA (GA), GroupB (GB), and GroupC (GC) are each requested to perform annotation following the workflow described in Sec. 3.3, and the leaders here only carry out result collections. We then sample 18 sets from the annotations of each group to conduct two-stage Cross-Check [1, 13], in which we first exchange the annotations of three groups in pairs and then label these samples again, as illustrated in Fig. 3 (b). These sets, each including 100 samples, are equally divided into two parts for two-stage Cross-Check (*i.e.*, sA , sB). Each stage has three sets for Neutral, two sets for Excitation, and one set for each of Sadness, Relaxation, Tension, as well as Fear. Afterwards, we evaluate the consistencies of intra-group and inter-group under the present allocations based on the results of Cross-Check_ sA . The ranges of S_a and S_r formulated as Eq. 2 and Eq. 3 below are from 0 to 1 and 0 to 70, respectively. The larger S_a and S_r indicate the increasing consistencies.

$$S_a = \frac{1}{n} \cdot \sum_{i=0}^{n-1} \left(\frac{1}{3 \cdot m} \cdot \sum_{j=1}^m c_j \right), \quad (2)$$

$$S_r = \frac{1}{c} \sum_{i=0}^{n-1} w_i \cdot (0.7 \cdot C_i + 0.3 \cdot (m - C_i - M_i)), \quad (3)$$

where n , m , and c denote the number of sets, samples per set, and emotional categories, respectively. c_j refers to the quantity of currently annotated categories of three annotators for one sample that are consistent with the previous category. $w_i \in \{\frac{1}{3} \mid 0 \leq i < 3, \frac{1}{2} \mid$

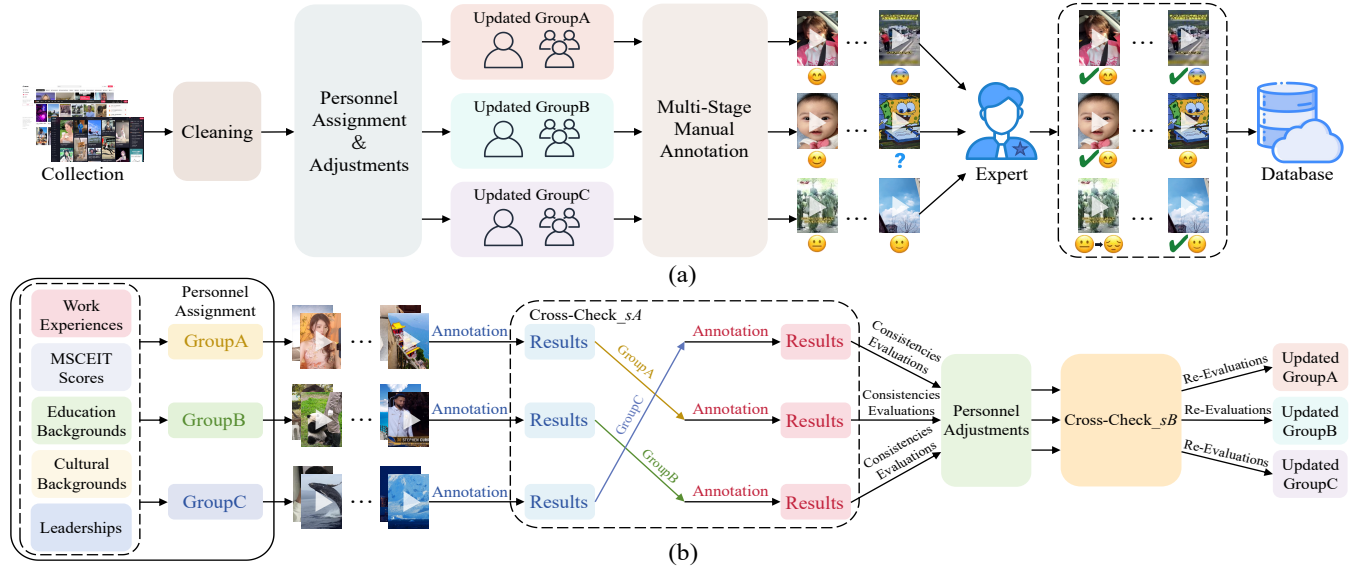


Figure 3: (a) The overall pipeline of dataset construction. (b) The detailed workflow of personnel assignment and adjustments.

Table 1: The evaluation results of consistencies of intra-group and inter-group (S_a and S_r) following Cross-Check.

Stage	GroupA		GroupB		GroupC	
	S_a	S_r	S_a	S_r	S_a	S_r
sA	0.52	52.55	0.53	48.78	0.55	54.54
sB	0.55	55.53	0.56	54.41	0.56	55.79

$3 \leq i < 5, 1 \leq i \leq 8$) represents the weight coefficient for each set, depending on the number of sets in each category. C_i stands for the samples consistent with previous annotations. M_i denotes the "more" samples, indicating the final label is indeterminate.

As shown in Tab. 1, S_a of the three groups achieve 0.52, 0.53, and 0.55, respectively. S_r stand at 52.55, 48.78, and 54.54, with GB scoring relatively low. Considering these observations, we perform targeted adjustments, then re-evaluate the consistencies after Cross-Check_sB. Following adjustments, S_a of GA and GB both rise by 0.03, and that of GC improves by 0.01. S_r of three groups increase by 2.98, 5.63, and 1.25, in which GB exhibits the highest improvement. These results demonstrate the effectiveness of our adjustments, indicating that we have finalized the personnel allocations that can be deployed for formal annotation. Note that the overall results of two-stage Cross-Check and the pseudocode of personnel adjustments strategy are detailed in the appendix.

3.3 Multi-Stage Manual Annotation

The setting of categories is essential for VEA datasets. We select the six emotions proposed by Plutchik in [35], since they have clearer boundaries and can better capture emotional changes evidenced by Russell's Circumplex Model [38]. The multi-stage manual annotation workflow combines member votes and leader evaluations, benefiting to alleviate the impact of subjectivities. Following [33], we adopt and extend the mapping table of emotion category-adjective to promote annotations, as shown in the appendix. Besides, we develop a labeling interface to boost the stimulation and engagement of annotators. Specifically, the leader distributes

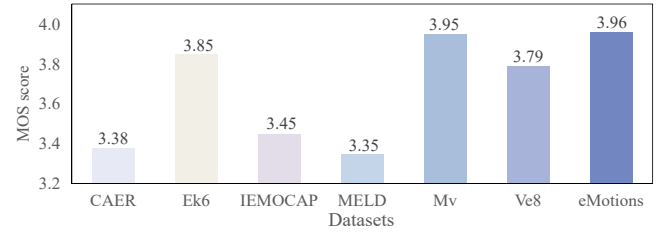


Figure 4: The MOS scores of six VEA datasets and our eMotions. Ek6: Ekman6. Mv: Music_video. Ve8: VideoEmotion8.

data, followed by three members undertaking annotations via the proposed mapping table. Meanwhile, members are asked to attach confidence scores to their annotations, and the average confidence score finally stands at 0.7. Next, the leader collects these annotations, leveraging a majority voting scheme to determine labels. If annotations from three members are all different (*i.e.*, samples labeled "more"), the leader will intervene in labeling. If a decisive majority of four votes emerges, the final labels can be directly determined. If consensus is still unreachable, leaders will exchange samples to facilitate decision-making. In five votes, a clear majority allows us to determine the final labels. If consensus continues to be inaccessible, the expert from BD Cloud will finalize the labels in re-review. After completing the annotation process, we calculate the overall Fleiss'kappa score, achieving $k > 0.45$.

3.4 Labeling Quality Evaluations

In this section, we conduct labeling quality evaluations for eMotions and six VEA datasets. Specifically, we first perform the random sampling of seven datasets, totaling 979 samples, based on the sample correction formula from [44]. We then employ four emotional annotation experts to independently evaluate the labeling quality of these datasets. The MOS scores [41] are utilized as the evaluation metric, in which the ratings from 1 to 5 represent the five levels of quality (*i.e.*, bad, poor, fair, good, excellent). Next, for each dataset, we average the assessments of four experts and regard the output

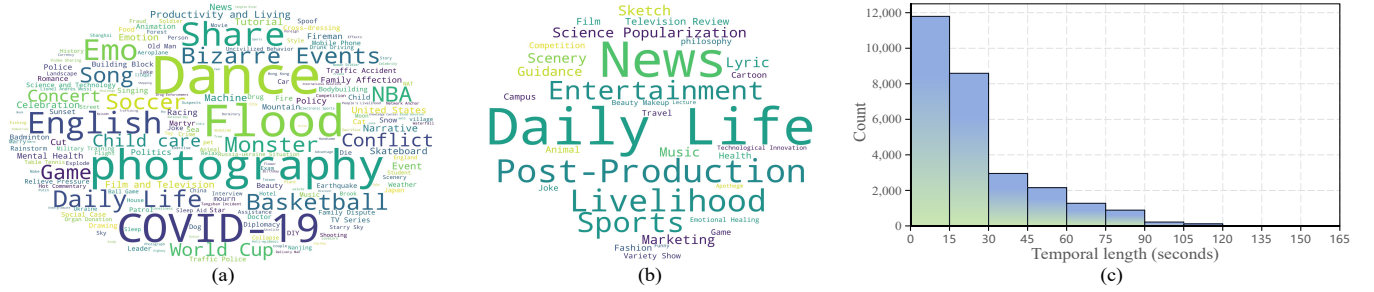


Figure 5: (a) & (b) Word clouds of topics and content types in eMotions. Larger text size indicates a higher frequency of occurrence. (c) Duration distribution of short-form videos in our dataset.

Table 2: The statistics of eMotions, detailing the number of videos and processed frames, along with the quantitative durations. The magnitude is 10^4 for "Total (s)" and "Frames".

Category	Videos	Total (s)	Shortest (s)	Longest (s)	Average (s)	Frames
Excitation	11,739	29.35	3.72	163.77	25.00	945.29
Fear	954	2.59	2.81	117.49	27.08	78.56
Neutral	8,795	24.97	2.46	150.93	28.39	815.11
Relaxation	2,214	5.24	5.06	117.05	23.69	163.80
Sadness	2,090	4.04	3.25	120.77	19.30	131.53
Tension	2,204	4.90	3.79	119.32	22.25	152.15
Overall	27,996	71.09	2.46	163.77	25.39	2,286.44

Table 3: The quantity and proportions of raw and labeled data across three SVs platforms.

Data Type	Douyin		Kuaishou		Tiktok		Sum
	No.	Ratio	No.	Ratio	No.	Ratio	
Raw	15,977	47.58%	10,000	29.78%	7,600	22.64%	33,577
Labeled	12,395	44.27%	8,264	29.52%	7,337	26.21%	27,996

as the final rating. Although the videos in Music_video [33] sourced from music recordings are easier to evoke emotions and the inherently unique challenges presented in eMotions, our dataset still ranks the first position, indicating the more reliable annotations compared with existing datasets, as shown in Fig. 4. These results verify the effect of our efforts in augmenting labeling quality.

3.5 Dataset Characteristics

We show the statistics of eMotions in Tab. 2, including the number of videos and processed frames for each category, as well as the quantitative durations. We observe that Excitation has the largest number of videos, while the negative emotions (*i.e.*, Fear, Sadness, Tension) have the smaller number of videos. In Tab. 3, we present the quantity and proportions of raw and labeled data across three SVs platforms. We figure out that the videos from Douyin and Kuaishou, two Chinese SVs platforms, account for the largest proportion.

We display the word clouds of topics and content types in Fig. 5 (a) and Fig. 5 (b). It can be seen that the topics mainly focus on daily events in our life, such as dance and photography, as well as the real-time events, such as COVID-19, flood. Content types are closely connected to human beings (*e.g.*, daily life, livelihood, news). Moreover, some topics and content types of SVs are consistent (*e.g.*, game, health). Fig. 5 (c) presents the distribution of SVs duration. We find that the durations mainly concentrate from 0 to 30 seconds, taking up 72.81% of the overall dataset. This indicates that SVs are concise, which can meet the needs of online users for quick dissemination

of web information. Besides, different from the human-centered VEA datasets (*e.g.*, [4, 37, 62]), eMotions originating from SVs is directed towards in-the-wild scenes, implying that the emotional elicitation requires the whole duration, not short clips of video.

3.6 Definitions of Two Variant Datasets

We build two variant datasets through targeted selections to meet various research needs. For eMotions_balanced, we randomly select samples from eMotions, in which 4,000 samples of Excitation, 3,000 samples of Neutral, and all the samples of the remaining categories. Regarding eMotions_test, we randomly select the corresponding proportion of samples based on the ratio of each emotional category in eMotions, totaling 5,000 samples. We detailedly show the statistics of two variant datasets in the appendix.

4 METHODOLOGY

4.1 Visual and Audio Representations

To tackle the inherent challenges of eMotions, we end-to-end learn audio-visual representations. Unlike [63, 65], we employ the Video Swin-Transformer (Video Swin-T) [30] as the visual backbone since it can capture more semantically relevant features. Specifically, let $\{(v_i, a_i)\}^b$ be a batch of b samples, in which v_i, a_i denote the video and audio in i -th sample. For v_i , we divide it into s segments of equal duration and randomly select T successive frames from each segment by keeping the temporal order, as the input snippets. For each snippet-level input $v_i^j \in \mathbb{R}^{T \times H \times W \times 3}$, we first project it into the patch features $v_i^j \in \mathbb{R}^{\frac{T}{2} \times \frac{H}{4} \times \frac{W}{4} \times 96}$, where H and W refer to the height and width of v_i . For the l -th stage in Video Swin-T, the input features can be represented as $F_v^l = \frac{T}{2} \times \frac{H}{2^{l+1}} \times \frac{W}{2^{l+1}} \times 2^{l-1}C$, $l \in \{1, 2, 3, 4\}$. For the first stage, a linear embedding layer is applied to project the dimension of patch features to C . The patch merging layers are then utilized in the remaining stages to progressively reduce the spatial size of feature maps. Moreover, the blocks in Video Swin-T deploy the novel 3D SW-MSA Module to capture global relations and model spatial-temporal correlations. The final representations of v_i comprise a series of snippet features $F_v(v_i) = \{f_v^1(v_i), f_v^2(v_i), \dots, f_v^s(v_i)\}$, and $f_v^j(v_i) \in \mathbb{R}^{\frac{T}{2} \times \frac{H}{32} \times \frac{W}{32} \times 8C}$.

For audio a_i , we obtain a successive descriptor a through MFCC. We then center-crop a to a fixed length of q and pad itself when necessary to get a' . Next, we divide a' along the time series length into s snippets via chunking and stacking, utilize ResNet34 [16] to output the final representations $F_a(a_i) = \{f_a^1(a_i), f_a^2(a_i), \dots, f_a^s(a_i)\}$, and

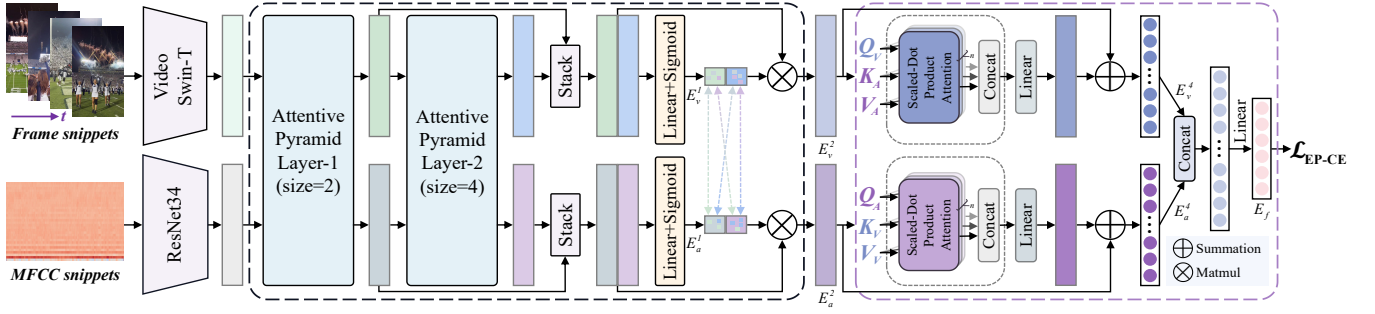


Figure 6: The overall illustration of AV-CANet. The Local-Global Fusion (LGF) Module consists of Local-level Interactive-Selective Fusion and Global-level Complementary Fusion Sub-Modules, framed by dashed lines in black and purple, respectively.

$f_a^p(a_i) \in \mathbb{R}^{H' \times W' \times C'}$, in which H' , W' , and C' denote the height, width, and final dimension, respectively.

Afterwards, we deploy poolings along spatial-temporal dimensions, followed by the fully connected layers to reshape F_v and F_a as $F_v \in \mathbb{R}^{s \times C_1}$ and $F_a \in \mathbb{R}^{s \times C_1}$.

4.2 Local-Global Fusion Module

We propose the LGF Module, including Local-level Interactive-Selective Fusion and Global-level Complementary Fusion (*i.e.*, LISF and GLCF) Sub-Modules, to progressively model the correlations of inter-modalities, thereby mitigating the local biases and collective information gaps caused by emotion inconsistency.

In the LISF Sub-Module, we first serially adopt two attentive pyramid layers [61], building upon the reformed Self-Attention (SA) and Cross-Modal Attention (CMA) blocks, to provide locally dense interactions of audio-visual features. Concretely, to facilitate interactions at multiple contextual scales in the pyramid layers, we set the fixed interaction window $s_t(F, d) = [F_{t-d}, \dots, F_{t+d}]$ by adding masks to regions that should not be involved, where d denotes the size for t^{th} snippet and $t \in [1, s]$, constraining the interacting size of blocks. With this fixed-size mechanism, the attention calculation of SA and CMA blocks at snippet-level can be formulated as:

$$SA(F_m, d) = Att(F_m W_q, s_t(F_m, d) W_k, s_t(F_m, d) W_v), \quad (4)$$

$$CMA(F_m, F_{\bar{m}}, d) = Att(F_m W_q, s_t(F_{\bar{m}}, d) W_k, s_t(F_{\bar{m}}, d) W_v), \quad (5)$$

$$Att(q, k, v) = softmax(qk^T / \sqrt{d_k})v, \quad (6)$$

where q , k , v , and $1/\sqrt{d_k}$ refer to queries, keys, values, and the scaling factor, W_* ($*$ $\in \{q, k, v\}$) are learnable parameters, modality $m \in \{a, v\}$. Subsequently, the reformed feed-forward layer, Layer-Norm [2], and residual connection are deployed to form the complete SA and CMA blocks.

When multiple attention heads are adopted, the outputs of SA and CMA blocks can be represented as:

$$F_s^m = c(Att_{sa}^1, \dots, Att_{sa}^n) W_0, \quad (7)$$

$$F_c^m = c(Att_{cma}^1, \dots, Att_{cma}^n) W_1, \quad (8)$$

where $c(\cdot)$ and n denote concatenation and the number of attention heads, W_0 and W_1 are learnable parameters. Besides, the parameters in CMA block are shared to facilitate local-level interactions.

For the parallel outputs of SA and CMA blocks, we first concatenate them and compute channel-wise attention scores to perform

refinement via a linear layer followed by a sigmoid function, then summation is used to output the local-aware audio-visual features:

$$F_m^l = \sigma(W_s \cdot c(F_s^m, F_c^m) + b_s) F_s^m + \sigma(W_c \cdot c(F_s^m, F_c^m) + b_c) F_c^m, \quad (9)$$

where $\sigma(\cdot)$ denotes sigmoid function, W_* and b_* ($*$ $\in \{s, c\}$) are the learnable parameters of linear layers.

Following [24, 61], the acasually dilated residual blocks are then adopted to amalgamatedly derive temporal semantics and perform positional enhancements. In the end, the densely interactive outputs $\{F_v^l, F_a^l\}_{l=1}^L$ for t^{th} snippet are preserved as pyramid-like features, in which $F_m^l \in \mathbb{R}^{1 \times C_1}$ and L is the number of pyramid layers.

To adaptively conduct selective integrations of pyramid features at snippet-level, we propose the Selectively Cross-Aggregative Integration Layer instead of simply using poolings. To be specific, for t^{th} snippet, we first stack $\{F_m^l\}_{l=1}^L$ along L to unify interactive features at multiple pyramid layers. The linear projection and sigmoid function are then performed to dynamically assign weights for different granularities, which can be formulated as:

$$E_m^1 = \sigma(W_a \cdot s(F_m^1, \dots, F_m^L) + b_a), \quad (10)$$

where $s(\cdot)$ refers to stacking operation. Afterwards, we deploy the CMA block without fixed-size window, where the number of head and dimension both are 1, to adaptively adjust the importance of audio-visual weights. In the end, the weighted summation of pyramid layers is conducted to output the compatibly integrated features E_m^2 . The formulation of above operations is given as follows:

$$E_m^2 = \sum_{l=1}^L s^l(F_m^1, \dots, F_m^L) \cdot Att^l(E_m^1 W_q, E_m^1 W_k, E_m^1 W_v). \quad (11)$$

So far, our model learns representations that are well-aware of local biases. To mitigate the collective information gaps, we introduce the GLCF Sub-Module, which facilitates correlated information capture of audio-visual features at global-level and outputs the final results. Specifically, we first utilize the globally unrestricted CMA block [51] with multiple attention heads to complementarily learn audio-visual representations at various levels and different degrees of correlations between snippets s . Then, concatenation is performed for non-local aggregations, *i.e.*,

$$E_m^3 = c(Att_{gca}^1, \dots, Att_{gca}^i (E_m^2 W_q, E_m^2 W_k, E_m^2 W_v), \dots, Att_{gca}^n) W_2. \quad (12)$$

Afterwards, the linear projection layers are deployed to enhance the focus on discriminative information and snippet-aware correlations. The residual connection is also utilized to benefit the free

Table 4: Performance comparisons of recent VEA methods and our AV-CANet on three eMotions-related datasets. We report the overall metrics of Accuracy (ACC) and Weighted Average F1-Score (WA-F1), as well as the ACC of each emotional category. EX: Excitation. FR: Fear. NU: Neutral. RE: Relaxation. SD: Sadness. TN: Tension. e_B: eMotions_balanced. e_T: eMotions_test. e_All: eMotions. Throughout this paper, we highlight the best performance in **bold and underline the second performance.**

Method	ACC of Each Emotional Category (%)												Evaluation Metrics (%)											
	EX			FR			NU			RE			SD			TN			ACC		WA-F1			
	e_B	e_T	e_All	e_B	e_T	e_All	e_B	e_T	e_All	e_B	e_T	e_All	e_B	e_T	e_All	e_B	e_T	e_All	e_B	e_T	e_All			
ResNet34 [16]	66.63	70.00	78.92	50.79	41.18	37.17	37.67	57.32	55.66	68.62	51.90	44.70	37.08	12.00	16.27	52.38	17.95	22.90	53.44	55.20	58.39	52.65	53.13	56.14
PANNS [21]	71.25	78.10	<u>83.48</u>	49.74	41.18	43.46	30.17	45.86	42.58	57.79	41.77	50.79	36.60	4.00	16.75	51.02	5.13	29.93	51.16	52.60	57.48	50.06	48.48	54.99
A ECAPA-TDNN [7]	69.13	<u>80.24</u>	84.63	42.93	29.41	29.32	36.83	39.81	47.24	49.21	31.65	42.66	55.02	36.00	23.68	38.78	14.10	13.38	50.99	53.50	57.52	50.45	50.92	54.55
Res2Net [11]	73.63	75.24	71.98	43.98	32.35	40.84	35.83	47.13	51.51	57.79	45.57	48.98	26.08	5.33	17.70	44.44	20.51	30.39	50.09	53.10	55.34	48.72	50.37	53.96
CAMPPlus [53]	69.00	73.03	78.62	40.31	41.18	34.56	36.50	48.09	49.91	65.46	51.90	48.08	38.28	10.67	13.88	48.53	25.32	18.14	52.26	54.00	56.09	51.37	52.06	53.51
V Video Swin-Transformer [30]	66.67	66.83	65.64	66.14	<u>61.76</u>	49.21	69.76	<u>80.25</u>	86.80	71.37	56.96	55.30	51.63	40.00	40.19	55.03	11.39	10.20	64.12	63.70	64.64	<u>64.31</u>	62.21	62.92
I3D [5]	69.84	68.74	71.48	74.87	64.71	52.36	62.83	80.89	80.66	70.20	59.49	51.92	51.67	37.33	42.58	51.02	6.33	13.15	63.28	<u>64.40</u>	65.41	63.68	<u>62.68</u>	63.90
SlowFast [9]	70.34	76.37	77.71	5.76	0.00	0.00	22.33	47.77	51.42	38.37	7.59	15.35	45.93	14.67	11.24	48.98	0.00	3.40	44.43	48.70	51.05	41.94	42.77	45.60
V CTEN [63]	65.00	74.22	73.51	37.17	38.24	28.80	45.83	61.46	65.87	69.07	54.43	45.82	52.15	32.00	30.62	36.28	7.59	6.12	53.58	59.00	58.89	53.02	56.94	56.53
Former-DFER [66]	64.85	74.46	69.97	41.80	38.24	39.79	36.01	50.32	65.55	58.57	26.58	51.69	43.36	24.00	39.71	51.68	26.58	10.43	51.64	54.30	59.16	51.38	52.56	57.67
TimeFormer [3]	68.84	70.88	78.90	74.35	55.88	51.31	<u>63.33</u>	75.48	73.09	73.81	40.51	47.18	57.89	28.00	34.45	48.75	8.86	4.31	64.18	61.30	64.43	64.32	59.17	61.62
DFER-CLIP [67]	59.40	67.48	69.55	84.29	50.00	92.38	45.49	53.44	57.12	<u>74.32</u>	57.14	73.56	63.98	<u>44.68</u>	67.60	51.42	<u>39.13</u>	<u>40.80</u>	58.82	58.90	64.33	59.04	56.96	63.07
C3D [49]	<u>72.84</u>	<u>76.61</u>	65.94	69.63	55.88	41.88	51.33	62.74	<u>82.76</u>	69.53	49.37	58.92	55.50	37.33	43.78	51.25	12.66	3.40	61.86	61.40	63.27	61.84	59.72	61.04
VAANet [65]	72.38	74.46	72.79	63.35	47.06	58.64	47.83	57.01	65.43	67.95	54.43	59.14	44.50	28.00	45.22	59.41	37.97	32.88	60.01	60.10	63.71	59.89	59.46	63.31
OGM-GE [34]	67.27	77.00	80.32	67.20	35.29	34.34	33.92	48.30	42.71	46.64	27.69	39.62	31.33	26.83	18.33	56.60	8.57	34.20	50.78	54.20	55.39	50.02	51.49	53.19
A+V MSAF [46]	60.33	63.43	71.57	54.77	44.83	51.32	41.30	60.52	65.06	70.95	37.18	60.92	52.36	26.39	37.03	47.80	15.28	12.33	54.69	53.73	60.93	54.51	52.70	59.51
MMCosine [56]	59.03	78.17	68.93	35.45	23.53	48.99	41.08	45.51	53.87	59.22	30.77	43.63	57.89	28.05	34.29	50.34	7.14	23.53	52.47	53.60	55.27	52.46	50.60	54.35
3D-ResNet50 + ResNet34 [15, 16]	72.50	68.02	77.73	69.63	35.29	60.21	49.17	69.43	59.24	72.69	<u>58.23</u>	60.50	55.74	36.00	36.36	55.78	17.72	41.04	62.53	60.20	63.98	62.31	59.04	63.45
ConvNeXt + CSP-DarkNet53 [29, 52]	66.25	77.33	78.36	<u>75.92</u>	50.00	66.49	46.17	62.74	61.46	69.30	50.63	57.11	65.55	34.67	54.55	65.08	35.44	33.11	62.91	63.20	65.62	62.87	62.33	65.01
AV-CANet	67.03	82.58	80.24	68.25	58.82	59.16	50.87	62.10	63.39	75.05	45.57	63.43	<u>65.16</u>	48.00	54.07	63.53	46.84	40.14	64.40	67.00	67.79	64.32	66.28	67.32

information flow and gradient propagation, followed by pooling layers along the snippet dimension to reshape features as $E_m^4 \in \mathbb{R}^{C^2}$:

$$E_m^4 = \delta \left(\left(W_g \cdot E_m^3 + b_g \right) + E_m^2 \right), \quad (13)$$

where $\delta(\cdot)$ denotes average pooling. In the end, we adopt the Mid-Concat fusion strategy, followed by a category-specific linear layer to output the final representations of our overall model, *i.e.*,

$$E_f = W_f \cdot c \left(E_m^4, E_m^4 \right) + b_f. \quad (14)$$

4.3 Emotion Polarity Enhanced CE Loss

Directly optimizing the traditional CE Loss could lead to misclassification due to the more significant semantic gaps and difficulties in learning emotion-related features. Inspired by [65], we develop the EP-CE Loss, which further considers the *neutral* polarity presented in eMotions and many VEA datasets [4, 23, 33]. Specifically, when the emotion polarity of prediction is different from the ground-truth, the $\gamma_{ep(y_i)}$ will function to weight model optimization. The EP-CE Loss can be defined as:

$$\mathcal{L}_{ep} = -\frac{1}{N} \sum_{i=1}^N \left(1 + \gamma_{ep(y_i)} \cdot s(y_i, \hat{y}_i) \right) \sum_{c=0}^{C-1} \beta_{[c=y_i]} \log p_{i,c}, \quad (15)$$

where C is the number of categories, $\beta_{[c=y_i]}$ is a binary indicator, and $p_{i,c}$ is the predicted probability that sample i belongs to category c . $\gamma_{ep(y_i)}$ refers to the coefficients for polarities that control the penalty extents. y_i and \hat{y}_i refer to the ground-truth and prediction. $s(y_i, \hat{y}_i)$ represents whether to add the penalties. When $ep(y_i) \neq ep(\hat{y}_i)$, $s(y_i, \hat{y}_i) = 1$, otherwise $s(y_i, \hat{y}_i) = 0$, where $ep(\cdot)$ maps the emotional category to its corresponding polarity.

Furthermore, to improve the training stability on large-scale dataset, we first deploy the deferred update strategy after every 4

Table 5: Performance comparisons of our LGF Module with advanced overall fusion methods.

Method	eMotions		Music_video		Ekman6	
	ACC	WA-F1	ACC	WA-F1	ACC	WA-F1
Vanilla	65.98	65.05	75.19	74.66	50.31	50.41
Self-Attention [51]	<u>67.21</u>	<u>66.72</u>	81.77	81.56	51.56	50.73
LGI-Former [47]	67.13	66.51	<u>82.03</u>	<u>82.08</u>	<u>53.75</u>	<u>53.20</u>
Sun et al. [48]	66.14	65.15	77.97	77.62	49.69	49.29
LGF Module	67.48	67.19	82.78	82.46	54.06	53.51

batches, then adopt the multi-task learning manner, which accumulates the loss of overall, visual and audio branches.

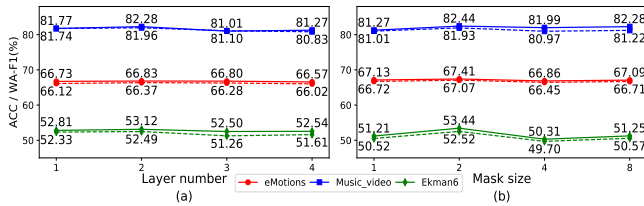
5 EXPERIMENTS

5.1 Main Results

Performance Comparisons. To demonstrate the effectiveness of proposed model, we compare with 19 baseline methods on three eMotions-related datasets, in which the modalities of compared baselines include audio (A), visual (V), and audio-visual (A+V), as illustrated in Tab. 4. We draw the following observations: (1) Visual features dominate audio-visual VEA, and the stronger visual architecture generally leads to more performance improvements. (2) Compared with other methods, AV-CANet exhibits relatively balanced performance across six emotions on three datasets, indicating that it can adeptly understand the emotions in SVs. (3) Benefit from the effective design of tackling challenges of eMotions, AV-CANet achieves superior performance across the overall metrics, exhibiting the improvements of 4.08% ACC and 4.01 WA-F1 on eMotions compared to VAANet [65]. Besides, we present the comparison results in terms of UAR and WAR across three datasets in the provided appendix.

Table 6: The overall performance comparisons of recent baseline methods and AV-CANet on Ekman6 (Ek6), VideoEmotion8 (Ve8), Music_video (Mv), and IEMOCAP (IE). EM: Evaluation metrics. *: The lab-controlled dataset. -: The results are not available.

Dataset	EM	A					V					A+V					Ours					
		[16]	[21]	[7]	[11]	[53]	[30]	[5]	[9]	[63]	[66]	[3]	[67]	[49]	[65]	[34]		[33]	[46]	[56]	[15, 16]	[29, 52]
Ek6	ACC	33.95	27.47	28.40	31.17	29.01	47.59	40.51	28.35	<u>53.44</u>	37.96	36.33	44.44	44.05	50.31	34.26	-	30.56	33.33	48.44	50.00	55.63
	WA-F1	32.17	21.77	28.21	29.64	29.03	49.44	42.10	21.92	<u>52.76</u>	36.88	34.34	43.81	42.84	49.65	33.10	-	25.35	33.08	47.57	49.33	55.44
Ve8	ACC	31.63	27.91	26.98	29.77	22.33	46.31	40.89	25.12	<u>47.66</u>	35.35	46.30	37.21	42.36	46.73	33.33	-	31.25	32.18	44.39	45.33	49.53
	WA-F1	29.11	23.06	23.20	27.12	23.59	45.77	41.34	16.06	<u>47.04</u>	29.10	45.65	29.32	42.02	43.92	32.12	-	28.56	26.82	43.21	45.23	48.24
Mv	ACC	72.73	63.38	69.95	65.91	70.71	74.68	64.05	50.13	76.20	60.51	78.23	79.49	62.78	78.99	57.32	<u>83.30</u>	63.38	58.59	73.42	75.70	84.81
	WA-F1	73.07	61.46	69.95	65.76	71.79	80.64	79.75	45.17	75.43	59.73	81.07	79.51	77.43	77.99	56.46	<u>84.00</u>	63.06	57.70	72.98	74.25	84.63
IE*	ACC	53.09	53.44	55.31	48.78	51.81	68.48	68.64	27.54	55.31	54.26	38.27	32.91	68.96	62.08	49.07	-	50.70	49.42	63.36	61.03	<u>68.73</u>
	WA-F1	52.45	52.83	55.17	47.36	50.88	67.44	67.99	16.67	54.96	54.18	31.81	16.29	<u>68.16</u>	61.86	48.82	-	49.76	49.42	63.12	60.26	68.73

**Figure 7: Ablation study in investigating the influence of different layer number and mask sizes on LGF Module. The solid and dashed lines denote ACC and WA-F1, respectively.**

In Tab. 6, the comparative results on four public VEA datasets show that our model performs favorably against recent VEA methods of different modalities, demonstrating its generalizability and robustness for various application-oriented VEA. Additionally, considering the observations in model performance across datasets, some VEA-oriented methods underperform the fine-tuned general models with large-scale pre-training, implying the importance of large-scale datasets for VEA [47, 48]. Note that in the appendix, we present more analysis and qualitative evaluations.

The Effectiveness of LGF Module. As shown in Tab. 5, we fairly compare our LGF Module with advanced overall fusion methods using the same backbones on three datasets. We figure out that the LGF Module consistently outperforms the advanced methods, which exceeds the second performance up to 0.75% ACC and 0.38 WA-F1, indicating its effectiveness. Besides, we replace the fusion modules of five audio-visual baselines with the LGF Module to further investigate its impact, as shown in the appendix.

5.2 Ablation Studies

We systematically conduct in-depth ablation studies to investigate the key factors of AV-CANet on three datasets. (1) We first examine the influence of different layer number in the LISF Sub-Module, as illustrated in Fig. 7 (a). We conclude that the number of pyramid layers is not directly proportional to the gains, as too many layers result in overly dense interactions at local-level, leading to increased complexity and instability. (2) Next, we evaluate how different mask sizes affect performance, as displayed in Fig. 7 (b). We observe that inappropriate mask sizes lead to performance declines, indicating that our model are sensitive to mask size. (3) We then investigate the impact of different fusion strategies in the GLCF Sub-Module of LGF Module. As shown in Tab. 7, adopting Mid-Concat fusion strategy across three datasets achieves the largest

Table 7: The ablation comparisons of five different fusion strategies in the GLCF Sub-Module. EW: Element-Wise.

Fusion Strategy	eMotions		Music_video		Ekman6	
	ACC	WA-F1	ACC	WA-F1	ACC	WA-F1
Gated [19]	67.39	67.35	80.51	80.26	50.94	50.45
EW-Multiply	64.44	63.97	76.71	76.44	48.44	47.17
Neural	66.52	66.12	82.03	81.75	53.44	52.34
Mid-Concat	67.48	67.19	82.78	82.46	54.06	53.51
Sum	66.49	66.17	81.77	81.64	50.94	50.18

Table 8: Ablation study for the LISF and GLCF Sub-Modules.

LG-CF Module	eMotions		Music_video		Ekman6	
	ACC	WA-F1	ACC	WA-F1	ACC	WA-F1
None	65.98	65.05	75.19	74.66	50.31	50.41
LISF	67.41	67.07	82.44	81.93	53.44	52.52
GLCF	67.08	66.41	81.89	81.00	51.88	51.30
LISF + GLCF	67.48	67.19	82.78	82.46	54.06	53.51

Table 9: The ablation comparisons of five different penalties for EP-CE Loss. Note that γ_{neu} doesn't function on Ekman6.

$\gamma_{pos} : \gamma_{neu} : \gamma_{neg}$	eMotions		Music_video		Ekman6	
	ACC	WA-F1	ACC	WA-F1	ACC	WA-F1
0.3 : 0.3 : 0.3	67.34	66.83	84.03	83.75	54.37	54.18
0.4 : 0.4 : 0.4	67.34	66.89	84.05	83.89	54.38	53.88
0.5 : 0.5 : 0.5	67.53	67.22	84.81	84.58	55.00	54.29
0.7 : 0.7 : 0.7	67.79	67.32	84.81	84.63	55.63	55.44

performance improvement of 0.94% Acc and 1.02 WA-F1, while EW-Multiply and Sum fusion strategies result in performance declines across all the datasets. The outcomes indicate that the adaptability of AV-CANet to different fusion strategies has crucial influence on performance. (4) Afterwards, we present the ablation explorations on the two sub-modules of LGF Module, as depicted in Tab. 8. From the results, we conclude that the joint use of two sub-modules leads to the highest improvement, demonstrating their superiority in correlations modeling of audio-visual cues. (5) Finally, we ablate the emotion polarities with different penalties, as shown in Tab. 9. We find that when $\gamma_{ep}(y_i) = 0.7$, AV-CANet consistently performs best across three datasets. We thus determine that larger penalties generally facilitate model to focus more on misclassified samples, while enhancing its capability in learning emotion-related representations. Besides, we observe that smaller penalties on large-scale dataset may confuse model learning, leading to slight declines.

6 CONCLUSION AND PROSPECTS

In this paper, we introduce eMotions, the first large-scale VEA dataset towards SVs. It comprises 27,996 videos labeled across six emotions, sourcing from three SVs platforms. Meanwhile, we make efforts to augment the labeling quality by alleviating the influence of subjectivities. Additionally, two variant datasets are provided through targeted data sampling. We also develop the baseline AV-CANet to tackle the inherent challenges of VEA towards SVs. Extensive experimental results on three eMotions-related and four public datasets verify the superiority of our model. We hope this work can serve as a foundation and inspire more research.

The granular divisions of audio facilitate models to output more refined representations, and the utilization of text overlays in SVs can promote the understanding of emotions, both indicating the potential trends of eMotions. Moreover, we focus on improving the limited cultural generalizability and long-tail distributions presented in eMotions for future developments.

ACKNOWLEDGMENTS

eMotions and its two variants will not be transferred to outside parties without permissions and can be only utilized for academic research. In particular, the datasets will not be included as a part of any commercial software package or product of any institution.

REFERENCES

- [1] Gavin Abercrombie, Verena Rieser, and Dirk Hovy. 2023. Consistency is Key: Disentangling Label Variation in Natural Language Processing with Intra-Annotator Agreement. *arXiv preprint arXiv:2301.10684* (2023).
- [2] Jimmy Lei Ba, Jamie Ryan Kiros, and Geoffrey E Hinton. 2016. Layer normalization. *arXiv preprint arXiv:1607.06450* (2016).
- [3] Gedas Bertasius, Heng Wang, and Lorenzo Torresani. 2021. Is space-time attention all you need for video understanding?. In *ICML*, Vol. 2. 4.
- [4] Carlos Busso, Murtaza Bulut, Chi-Chun Lee, Abe Kazemzadeh, Emily Mower, Samuel Kim, Jeannette N Chang, Sungbok Lee, and Shrikanth S Narayanan. 2008. IEMOCAP: Interactive emotional dyadic motion capture database. *Language resources and evaluation* 42 (2008), 335–359.
- [5] Joao Carreira and Andrew Zisserman. 2017. Quo vadis, action recognition? a new model and the kinetics dataset. In *Proceedings of the IEEE Conference on Computer Vision and Pattern Recognition*. 6299–6308.
- [6] Kateryna Chumachenko, Alexandros Iosifidis, and Moncef Gabbouj. 2022. Self-attention fusion for audiovisual emotion recognition with incomplete data. In *2022 26th International Conference on Pattern Recognition (ICPR)*. IEEE, 2822–2828.
- [7] Brecht Desplanques, Jenthe Thienpondt, and Kris Demuynck. 2020. Ecapadnn: Emphasized channel attention, propagation and aggregation in tdnn based speaker verification. *arXiv preprint arXiv:2005.07143* (2020).
- [8] Abhinav Dhall, Roland Goecke, Simon Lucey, and Tom Gedeon. 2012. Collecting Large, Richly Annotated Facial-Expression Databases from Movies. *IEEE Multimedia* 19, 3 (2012), 0034.
- [9] Christoph Feichtenhofer, Haoqi Fan, Jitendra Malik, and Kaiming He. 2019. Slow-fast networks for video recognition. In *Proceedings of the IEEE/CVF international conference on computer vision*. 6202–6211.
- [10] Ivar Frisch and Mario Giulianelli. 2024. LLM Agents in Interaction: Measuring Personality Consistency and Linguistic Alignment in Interacting Populations of Large Language Models. *arXiv preprint arXiv:2402.02896* (2024).
- [11] Shang-Hua Gao, Ming-Ming Cheng, Kai Zhao, Xin-Yu Zhang, Ming-Hsuan Yang, and Philip Torr. 2019. Res2net: A new multi-scale backbone architecture. *IEEE transactions on pattern analysis and machine intelligence* 43, 2 (2019), 652–662.
- [12] Hatice Gunes and Massimo Piccardi. 2006. A bimodal face and body gesture database for automatic analysis of human nonverbal affective behavior. In *18th International conference on pattern recognition (ICPR'06)*, Vol. 1. IEEE, 1148–1153.
- [13] Kevin A Hallgren. 2012. Computing inter-rater reliability for observational data: an overview and tutorial. *Tutorials in quantitative methods for psychology* 8, 1 (2012), 23.
- [14] Alan Hanjalic and Li-Qun Xu. 2005. Affective video content representation and modeling. *IEEE transactions on multimedia* 7, 1 (2005), 143–154.
- [15] Kensho Hara, Hirokatsu Kataoka, and Yutaka Satoh. 2018. Can spatiotemporal 3d cnns retrace the history of 2d cnns and imagenet?. In *Proceedings of the IEEE conference on Computer Vision and Pattern Recognition*. 6546–6555.
- [16] Kaiming He, Xiangyu Zhang, Shaoqing Ren, and Jian Sun. 2016. Deep residual learning for image recognition. In *Proceedings of the IEEE conference on computer vision and pattern recognition*. 770–778.
- [17] Xingxun Jiang, Yuan Zong, Wenming Zheng, Chuangao Tang, Wanchuang Xia, Cheng Lu, and Jiateng Liu. 2020. Dfew: A large-scale database for recognizing dynamic facial expressions in the wild. In *Proceedings of the 28th ACM international conference on multimedia*. 2881–2889.
- [18] Yu-Gang Jiang, Baohan Xu, and Xiangyang Xue. 2014. Predicting emotions in user-generated videos. In *Proceedings of the AAAI conference on artificial intelligence*, Vol. 28.
- [19] Douwe Kiela, Edouard Grave, Armand Joulin, and Tomas Mikolov. 2018. Efficient large-scale multi-modal classification. In *Proceedings of the AAAI conference on artificial intelligence*, Vol. 32.
- [20] Dimitrios Kollias and Stefanos Zafeiriou. 2018. Aff-wild2: Extending the aff-wild database for affect recognition. *arXiv preprint arXiv:1811.07770* (2018).
- [21] Qiuqiang Kong, Yin Cao, Turab Iqbal, Yuxuan Wang, Wenwu Wang, and Mark D Plumbley. 2020. Panns: Large-scale pretrained audio neural networks for audio pattern recognition. *IEEE/ACM Transactions on Audio, Speech, and Language Processing* 28 (2020), 2880–2894.
- [22] Liliya Lavitas, Olivia Redfield, Allen Lee, Daniel Fletcher, Matthias Eck, and Sunil Janardhanan. 2021. Annotation quality framework-accuracy, credibility, and consistency. In *NEURIPS 2021 Workshop for Data Centric AI*.
- [23] Jiyoung Lee, Seungryong Kim, Sunok Kim, Jungin Park, and Kwanghoon Sohn. 2019. Context-aware emotion recognition networks. In *Proceedings of the IEEE/CVF international conference on computer vision*. 10143–10152.
- [24] Shijie Li, Yazan Abu Farha, Yun Liu, Ming-Ming Cheng, and Juergen Gall. 2020. Ms-tcn++: Multi-stage temporal convolutional network for action segmentation. *IEEE transactions on pattern analysis and machine intelligence* 45, 6 (2020), 6647–6658.
- [25] Zheng Lian, Haiyang Sun, Licai Sun, Zhuofan Wen, Siyuan Zhang, Shun Chen, Hao Gu, Jinming Zhao, Ziyang Ma, Xie Chen, et al. 2024. MER 2024: Semi-Supervised Learning, Noise Robustness, and Open-Vocabulary Multimodal Emotion Recognition. *arXiv preprint arXiv:2404.17113* (2024).
- [26] Zheng Lian, Licai Sun, Mingyu Xu, Haiyang Sun, Ke Xu, Zhuofan Wen, Shun Chen, Bin Liu, and Jianhua Tao. 2023. Explainable multimodal emotion reasoning. *arXiv preprint arXiv:2306.15401* (2023).
- [27] Shengzhe Liu, Xin Zhang, and Jufeng Yang. 2022. SER30K: A large-scale dataset for sticker emotion recognition. In *Proceedings of the 30th ACM International Conference on Multimedia*. 33–41.
- [28] Yuanyuan Liu, Wei Dai, Chuanxu Feng, Wenbin Wang, Guanghao Yin, Jiabei Zeng, and Shiguang Shan. 2022. Mafw: A large-scale, multi-modal, compound affective database for dynamic facial expression recognition in the wild. In *Proceedings of the 30th ACM International Conference on Multimedia*. 24–32.
- [29] Zhuang Liu, Hanzi Mao, Chao-Yuan Wu, Christoph Feichtenhofer, Trevor Darrell, and Saining Xie. 2022. A convnet for the 2020s. In *Proceedings of the IEEE/CVF conference on computer vision and pattern recognition*. 11976–11986.
- [30] Ze Liu, Jia Ning, Yue Cao, Yixuan Wei, Zheng Zhang, Stephen Lin, and Han Hu. 2022. Video swin transformer. In *Proceedings of the IEEE/CVF conference on computer vision and pattern recognition*. 3202–3211.
- [31] John D Mayer, Peter Salovey, and David R Caruso. 2002. Mayer-Salovey-Caruso emotional intelligence test (MSCEIT) users manual. (2002).
- [32] Bogdan Mocanu, Ruxandra Tapu, and Titus Zaharia. 2023. Multimodal emotion recognition using cross modal audio-video fusion with attention and deep metric learning. *Image and Vision Computing* 133 (2023), 104676.
- [33] Yagya Raj Pandeya and Joonwhoan Lee. 2021. Deep learning-based late fusion of multimodal information for emotion classification of music video. *Multimedia Tools and Applications* 80 (2021), 2887–2905.
- [34] Xiaokang Peng, Yake Wei, Andong Deng, Dong Wang, and Di Hu. 2022. Balanced multimodal learning via on-the-fly gradient modulation. In *Proceedings of the IEEE/CVF Conference on Computer Vision and Pattern Recognition*. 8238–8247.
- [35] Robert Plutchik. 1994. *The psychology and biology of emotion*. HarperCollins College Publishers.
- [36] Soujanya Poria, Erik Cambria, Devamanyu Hazarika, Navonil Majumder, Amir Zadeh, and Louis-Philippe Morency. 2017. Context-dependent sentiment analysis in user-generated videos. In *Proceedings of the 55th annual meeting of the association for computational linguistics (volume 1: Long papers)*. 873–883.
- [37] Soujanya Poria, Devamanyu Hazarika, Navonil Majumder, Gautam Naik, Erik Cambria, and Rada Mihalcea. 2018. Meld: A multimodal multi-party dataset for emotion recognition in conversations. *arXiv preprint arXiv:1810.02508* (2018).
- [38] Jonathan Posner, James A Russell, and Bradley S Peterson. 2005. The circumplex model of affect: An integrative approach to affective neuroscience, cognitive development, and psychopathology. *Development and psychopathology* 17, 3 (2005), 715–734.
- [39] R Gnana Praveen, Patrick Cardinal, and Eric Granger. 2023. Audio-visual fusion for emotion recognition in the valence-arousal space using joint cross-attention. *IEEE Transactions on Biometrics, Behavior, and Identity Science* (2023).
- [40] Alec Radford, Jong Wook Kim, Chris Hallacy, Aditya Ramesh, Gabriel Goh, Sandhini Agarwal, Girish Sastry, Amanda Askell, Pamela Mishkin, Jack Clark,

- et al. 2021. Learning transferable visual models from natural language supervision. In *International conference on machine learning*. PMLR, 8748–8763.
- [41] Flávio Ribeiro, Dinei Florencio, and Vitor Nascimento. 2011. Crowdsourcing subjective image quality evaluation. In *2011 18th IEEE International Conference on Image Processing*. IEEE, 3097–3100.
- [42] Liam Schoneveld, Alice Othmani, and Hazem Abdelkawy. 2021. Leveraging recent advances in deep learning for audio-visual emotion recognition. *Pattern Recognition Letters* 146 (2021), 1–7.
- [43] Dagmar Schuller and Björn W Schuller. 2018. The age of artificial emotional intelligence. *Computer* 51, 9 (2018), 38–46.
- [44] Ajay S Singh and Micah B Masuku. 2014. Sampling techniques & determination of sample size in applied statistics research: An overview. *International Journal of economics, commerce and management* 2, 11 (2014), 1–22.
- [45] Paweł Sobkowicz, Michael Kaschesky, and Guillaume Bouchard. 2012. Opinion mining in social media: Modeling, simulating, and forecasting political opinions in the web. *Government information quarterly* 29, 4 (2012), 470–479.
- [46] Lang Su, Chuqing Hu, Guofa Li, and Dongpu Cao. 2020. Msaf: Multimodal split attention fusion. *arXiv preprint arXiv:2012.07175* (2020).
- [47] Licai Sun, Zheng Lian, Bin Liu, and Jianhua Tao. 2023. Mae-dfer: Efficient masked autoencoder for self-supervised dynamic facial expression recognition. In *Proceedings of the 31st ACM International Conference on Multimedia*. 6110–6121.
- [48] Licai Sun, Zheng Lian, Bin Liu, and Jianhua Tao. 2024. HiCMAE: Hierarchical Contrastive Masked Autoencoder for Self-Supervised Audio-Visual Emotion Recognition. *Information Fusion* 108 (2024), 102382.
- [49] Du Tran, Lubomir Bourdev, Rob Fergus, Lorenzo Torresani, and Manohar Paluri. 2015. Learning spatiotemporal features with 3d convolutional networks. In *Proceedings of the IEEE international conference on computer vision*. 4489–4497.
- [50] Minh Tran and Mohammad Soleymani. 2022. A pre-trained audio-visual transformer for emotion recognition. In *ICASSP 2022-2022 IEEE International Conference on Acoustics, Speech and Signal Processing (ICASSP)*. IEEE, 4698–4702.
- [51] Ashish Vaswani, Noam Shazeer, Niki Parmar, Jakob Uszkoreit, Llion Jones, Aidan N Gomez, Lukasz Kaiser, and Illia Polosukhin. 2017. Attention is all you need. *Advances in neural information processing systems* 30 (2017).
- [52] Chien-Yao Wang, Hong-Yuan Mark Liao, Yueh-Hua Wu, Ping-Yang Chen, Jun-Wei Hsieh, and I-Hau Yeh. 2020. CSPNet: A new backbone that can enhance learning capability of CNN. In *Proceedings of the IEEE/CVF conference on computer vision and pattern recognition workshops*. 390–391.
- [53] Hui Wang, Siqi Zheng, Yafeng Chen, Luyao Cheng, and Qian Chen. 2023. CAM++: A Fast and Efficient Network For Speaker Verification Using Context-Aware Masking. *arXiv preprint arXiv:2303.00332* (2023).
- [54] Kai Wang, Xiaojiang Peng, Jianfei Yang, Shijian Lu, and Yu Qiao. 2020. Suppressing uncertainties for large-scale facial expression recognition. In *Proceedings of the IEEE/CVF conference on computer vision and pattern recognition*. 6897–6906.
- [55] Baohan Xu, Yanwei Fu, Yu-Gang Jiang, Boyang Li, and Leonid Sigal. 2016. Video emotion recognition with transferred deep feature encodings. In *proceedings of the 2016 ACM on international conference on multimedia retrieval*. 15–22.
- [56] Ruize Xu, Ruoxuan Feng, Shi-Xiong Zhang, and Di Hu. 2023. MMCosine: Multimodal Cosine Loss Towards Balanced Audio-Visual Fine-Grained Learning. In *ICASSP 2023-2023 IEEE International Conference on Acoustics, Speech and Signal Processing (ICASSP)*. IEEE, 1–5.
- [57] Fanglei Xue, Zichang Tan, Yu Zhu, Zhongsong Ma, and Guodong Guo. 2022. Coarse-to-fine cascaded networks with smooth predicting for video facial expression recognition. In *Proceedings of the IEEE/CVF Conference on Computer Vision and Pattern Recognition*. 2412–2418.
- [58] Jingyuan Yang, Jiawei Feng, and Hui Huang. 2024. EmoGen: Emotional Image Content Generation with Text-to-Image Diffusion Models. In *Proceedings of the IEEE/CVF Conference on Computer Vision and Pattern Recognition*. 6358–6368.
- [59] Jingyuan Yang, Jie Li, Leida Li, Xiumei Wang, and Xinbo Gao. 2021. A circular-structured representation for visual emotion distribution learning. In *Proceedings of the IEEE/CVF Conference on Computer Vision and Pattern Recognition*. 4237–4246.
- [60] Quanzeng You, Jiebo Luo, Hailin Jin, and Jianchao Yang. 2016. Building a large scale dataset for image emotion recognition: The fine print and the benchmark. In *Proceedings of the AAAI conference on artificial intelligence*, Vol. 30.
- [61] Jiashuo Yu, Ying Cheng, Rui-Wei Zhao, Rui Feng, and Yuejie Zhang. 2022. Mm-pyramid: Multimodal pyramid attentional network for audio-visual event localization and video parsing. In *Proceedings of the 30th ACM international conference on multimedia*. 6241–6249.
- [62] AmirAli Bagher Zadeh, Paul Pu Liang, Soujanya Poria, Erik Cambria, and Louis-Philippe Morency. 2018. Multimodal language analysis in the wild: Cmu-mosei dataset and interpretable dynamic fusion graph. In *Proceedings of the 56th Annual Meeting of the Association for Computational Linguistics*. 2236–2246.
- [63] Zhicheng Zhang, Lijuan Wang, and Jufeng Yang. 2023. Weakly Supervised Video Emotion Detection and Prediction via Cross-Modal Temporal Erasing Network. In *Proceedings of the IEEE/CVF Conference on Computer Vision and Pattern Recognition*. 18888–18897.
- [64] Zhicheng Zhang, Pancheng Zhao, Eunil Park, and Jufeng Yang. 2024. Mart: Masked affective representation learning via masked temporal distribution distillation. In *Proceedings of the IEEE/CVF Conference on Computer Vision and Pattern Recognition*. 12830–12840.
- [65] Sicheng Zhao, Yunsheng Ma, Yang Gu, Jufeng Yang, Tengfei Xing, Pengfei Xu, Runbo Hu, Hua Chai, and Kurt Keutzer. 2020. An end-to-end visual-audio attention network for emotion recognition in user-generated videos. In *Proceedings of the AAAI Conference on Artificial Intelligence*, Vol. 34. 303–311.
- [66] Zengqun Zhao and Qingshan Liu. 2021. Former-dfer: Dynamic facial expression recognition transformer. In *Proceedings of the 29th ACM International Conference on Multimedia*. 1553–1561.
- [67] Zengqun Zhao and Ioannis Patras. 2023. Prompting visual-language models for dynamic facial expression recognition. *arXiv preprint arXiv:2308.13382* (2023).
- [68] Hengshun Zhou, Debin Meng, Yuanyuan Zhang, Xiaojiang Peng, Jun Du, Kai Wang, and Yu Qiao. 2019. Exploring emotion features and fusion strategies for audio-video emotion recognition. In *2019 International conference on multimodal interaction*. 562–566.